ACES
DOI: 10.1002/asia.201403085
CHEMISTRY
AN ASIAN JOURNAL
Communication

Supercapacitors

Ultrathin Cerium Orthovanadate Nanobelts for High-Performance Flexible All-Solid-State Asymmetric Supercapacitors

Junzhi He,[a] Junhong Zhao,[a] Zhen Run,[a] Mengjun Sun,[a] and Huan Pang*[a, b]

Abstract: Ultrathin $CeVO_4$ nanobelts were successfully synthesized by a hydrothermal method. The thickness of a single nanobelt is about 2.4 nm, which can effectively shorten the ion diffusion and fasten the charge pathway. More importantly, ultrathin $CeVO_4$ nanobelts and graphene are easily assembled as a flexible all-solid-state asymmetric device, which shows a highly flexible property and achieves a maximum energy density of 0.78 mW h cm^{-3} and a high life cycle of $>$6000 cycles.

Supercapacitors (SCs) are a new kind of charge storage device which can be used for digital cameras, communication devices, mobile phones, electric tools, electric hybrid vehicles, pulse laser technique, uninterruptible power supplies for computers, and energy storage for solar cells.[1–6] However, to meet the increasing energy demands for next-generation portable and flexible devices, the energy density of SCs should be substantially increased to afford enough power density and cycle life.[7] The energy density (E) of a SC device increases with the increase of the device capacitance (C) and the cell voltage (U) based on the equation $E = 1/2\ CU^2$.[8] Though organic (vs. aqueous) electrolytes can effectively increase the cell voltage (up to $\approx$3 V),[9–11] they usually have poor ionic conductivity, high cost, and high toxicity, which could limit their wide application. Asymmetric supercapacitors (ASCs) with a battery-type Faradaic electrode as energy source and a capacitive electrode as a power source are a promising alternative due to the use of aqueous electrolytes that have higher ionic conductivities and are more environmentally friendly.[8,12–16] Intensive efforts have been devoted to explore various ASC systems,[8,12–18] such as graphene-MnO_2//activated carbon nanofibers,[8] $Ni(OH)_2$-graphene and graphene,[16] V_2O_5//active carbon,[17] and MnO_2//FeOOH.[18] However, aqueous ASC device fabrication usually requires high-cost encapsulation techniques to avoid the possible leakage of electrolytes, which makes small and flexible devices hard to obtain. Due to their small size, light weight, ease of handing, excellent reliability, and a wider range of operating temperatures, solid-state SCs are advantageous compared with conventional SCs,[19–25] holding great promise for flexible and wearable electronics. However, there are only few reports about the fabrication of solid-state ASCs. Recently, Lu et al. have successfully reported a solid-state ASC based on H-TiO_2@MnO_2//H-TiO_2@C core–shell nanowires.[23] The challenge to fabricate low-cost, high-performance solid-state ASCs.

Over the past years, cerium(III) orthovanadate ($CeVO_4$) nanostructures as one important member of metal orthovanadates have been widely investigated, as they may find use as next-generation catalysts, solar cells, magnetic and optoelectronic nanodevices, and biochemical labels.[26–29] However, there are no reports using $CeVO_4$ nanostructures as electrode materials for electrochemical capacitors. Here, we report on the hydrothermal synthesis of ultrathin $CeVO_4$ nanobelts and their application as high-performance, flexible, all-solid-state asymmetric supercapacitors. More importantly, the electrochemical results show that the assembled ultrathin $CeVO_4$ nanobelt//graphene ASCs achieve a maximum energy density of 0.78 mW h cm^{-3}, which is higher than the values of most reported solid-state SCs. Furthermore, the $CeVO_4$ nanobelts have an efficient cycle ability for 6000 cycles, which makes them as one of the most promising candidates for high-performance, flexible, solid-state asymmetric supercapacitors in the field of energy storage devices.

Figure 1a shows the XRD pattern for the as-prepared samples. All diffraction peaks in the experimental pattern can be indexed to pure $CeVO_4$ phase (JCPDS No-72-0282). No peaks from other phases have been detected, thus indicating the high purity of the product. Figure 1b shows a typical scanning electron microscopy (SEM) image of the as-synthesized $CeVO_4$ nanobelts obtained at 200 °C for 5 h. The overview image shows that the nanobelts have a uniform diameter of 25 nm along their entire length, which can be up to tens of micrometers. Moreover, these nanobelts are interconnected to form a porous network architecture, which might improve the diffusion of ions and electrolytes. The morphology and structure of the $CeVO_4$ nanobelts were further analyzed by transmission electron microscopy (TEM) and selected-area electron diffraction (SAED). The TEM image in Figure 1c shows that the diameters of the nanobelts are around 25 nm, which is consistent

[a] J. He, Dr. J. Zhao, Z. Run, M. Sun, Prof. H. Pang
College of Chemistry and Chemical Engineering
Anyang Normal University
Anyang, 455002, Henan (P. R. China)
Fax: (+86) 0372-2900213

[b] Prof. H. Pang
State Key Laboratory of Coordination Chemistry
Nanjing University
Nanjing, 210093, Jiangsu (P. R. China)
E-mail: huanpangchem@hotmail.com
Homepage: http://huanpangchem.wix.com/advanced-material

Supporting information for this article is available on the WWW under http://dx.doi.org/10.1002/asia.201403085.

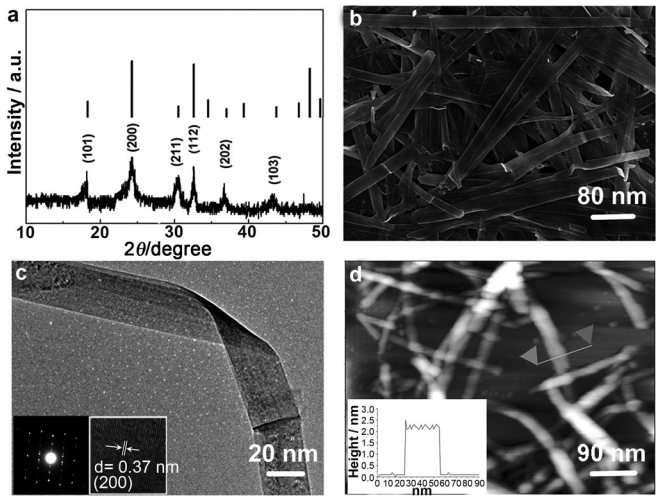

Figure 1. a) XRD patterns of an as-prepared $CeVO_4$ sample and JCPDS No. 72-0282 (top), b) FE-SEM image, c) TEM image (insets: HRTEM image and corresponding SAED pattern), and d) AFM image (inset: height of the cross section marked by arrowheads in panel d) of the as-prepared sample.

with the observation in the SEM image. From the SAED pattern of an individual nanobelt in the left inset of Figure 1 c, one can see that the nanobelt is structurally uniform and can described as a single crystal. The high-resolution TEM image (Figure 1 c, right inset) taken near the dodecahedral edges displays distinct lattice fringes with a d spacing of 0.37 nm, which is in good agreement with the (200) lattice planes of $CeVO_4$. The thickness of a single nanobelt was measured by the AFM image shown in Figure 1 d. From the AFM result (the inset in Figure 1 d), the thickness of the single nanobelt is determined to be about 2.4 nm. This ultrathin property can effective shorten the distance of ion difussion.

To gain further insight into the specific surface area and pore size distribution of the ultrathin $CeVO_4$ nanobelts, Brunauer–Emmett–Teller (BET) measurements were performed. The ultrathin $CeVO_4$ nanobelts show a distinct hysteresis in the range of about 0.7–1.0 P/P_0 (Supporting Information, Figure S1 a), indicating the presence of mesopores, possibly formed by the interconnected stacking of nanobelts. The BET surface area of the ultrathin $CeVO_4$ nanobelt is 108 $m^2 g^{-1}$. The corresponding Barrett–Joyner–Halenda (BJH) pore size distribution curve shows that the pore size is uniform (Supporting Information, Figure S1b, inset), within the range of mesopores. These porous structures not only result in high surface areas but also provide good electrolyte access. The ultrathin $CeVO_4$ nanobelts offer a stable structure for intercalatation/extraction of ions into/out of its structure, which might improve the cycle life of the electrode.

Figure 2 a shows the cyclic voltammogram (CV) curves of ultrathin $CeVO_4$ nanobelts in the potential range of −0.2 to 0.7 V (vs. SCE) in 1.0 M LiCl electrolyte solution at scan rates of 5–50 mV s^{-1} in a conventional three-electrode system. As shown, the current response increased with the scan rate, and the shapes are different from that of electric double-layer capacitance, suggesting that the capacity mainly results from pseudocapacitive capacitance. We also propose the reversible redox reactions in the as-prepared electrode:

$$HS\text{-}Ce^{III} + OH^-_{sol} \Leftrightarrow HS\text{-}(OH^-)Ce^{IV} + e^- \quad (1)$$

where HS stands for vanadate group [-VO_4].

Figure 2 b shows chronopotentiometry (CP) curves at different current densities. The symmetrical characteristic of charging/discharging curves is good, which signifies that the excellent electrochemical capability and redox process are reversible in the ultrathin $CeVO_4$ nanobelt electrode. The relationship between the specific capacitances calculated by the CP curves and current densities is also given in Figure 2 b. Based on the CP curves, the ultrathin $CeVO_4$ nanobelt electrode has a large specific capacitance that reaches up to 605 F g^{-1} at a cur-

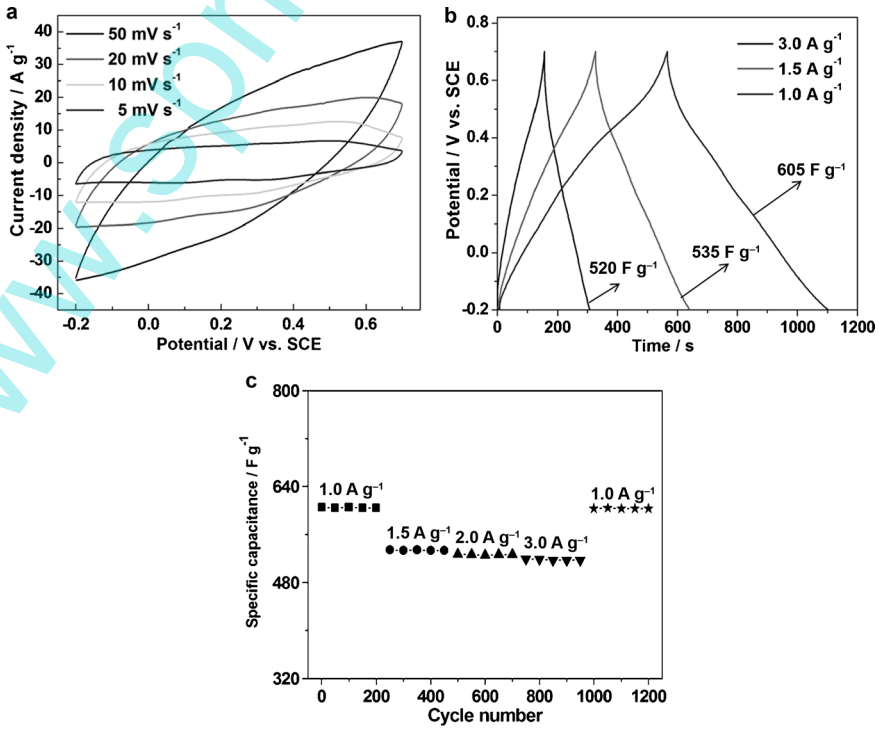

Figure 2. a) Cyclic voltammetry measurements carried out using the ultrathin $CeVO_4$ nanobelt electrode in 1.0 M LiCl at room temperature within the range of −0.20 to 0.70 V at a scan rate of 5–50 mV s^{-1}. b) Galvanostatic charge–discharge curves at current densities of 1.0, 1.5, and 3.0 A g^{-1}. c) Cycle life performance tests at different current densities.

rent density of 1.0 A g^{-1} and remains at 520 F g^{-1} even at 3.0 A g^{-1}.

The cycling performance of the ultrathin $CeVO_4$ nanobelt electrode at different current densities (1.0, 1.5, 2.0, 3.0, and 1.0 A g^{-1}) is shown in Figure 2c. One can see that increasing the current density from 1.0 A g^{-1} to 3.0 A g^{-1} resulted in a reduction of the capacity from 605 F g^{-1} to 518 F g^{-1}, while the stable cycling performance at each current density is still maintained, further confirming the stability of the electrode.

With the aim to develop flexible power sources, a flexible solid-state asymmetric supercapacitor was further fabricated using the ultrathin $CeVO_4$ nanobelts and graphene ($CeVO_4$ nanobelts//graphene) as active materials according to our previous method.[25] CV curves of the flexible solid-state asymmetric supercapacitor at different scan rates (ranging from 5 to 100 mV s^{-1}) were measured below 1.9 V (Figure 3a). Unlike the three-electrode electrochemical feature of the ultrathin $CeVO_4$ nanobelt electrode, the ASC device displays a quasi-rectangular CV geometry with weak redox peaks, indicating a combination of both pseudocapacitive and electric double-layer capacitor properties at all scan rates. Moreover, at a scan rate as high as 100 mV s^{-1} and a maximum cell voltage of 1.9 V, the shape of the CV curve was still well maintained, suggesting a good rate capability of the flexible solid-state ASC.

Galvanostatic charge–discharge curves of the flexible solid-state ASC at various current densities are shown in Figure 3b. The corresponding specific capacitance is shown in Figure 3b, and it reached 155.8 mF cm^{-2} at a current density of 0.50 mA cm^{-2}. In order to test the flexibility of our solid-state ASC, it was bent to different angles (Figure 3c), while the corresponding electrochemical tests were conducted. CV measurements were conducted at a scan rate of 30 mV s^{-1} with two bending angles (90° and 180°), as shown in Figure 3c. Only small changes of the CV curves were observed with different bending angles. Remarkably, throughout the bending processes, the specific capacitance of the device was maintained. The calculated decay ratio is 1.2% at 90° bending and 1.4% at 180° bending compared with that of the normal condition. In fact, we have measured the performance of the as-prepared device after bending for 300 times (Supporting Information, Figure S2b). The as-prepared device shows only 3.1% reduction upon bending to different angles for 300 times. The flexible characteristic is shown in some optical photos (Supporting Information, Figure S3 and Figure 3c, inset). The variation of open cell voltages under different bending modes is listed in Table S1 in the Supporting Information. It is seen that the open cell voltages changed little under different bending modes, again confirming the good flexible ability of the as-prepared ASC device. Moreover, it is found that the flexible solid-state ASC can maintain the initial value of the specific capacitance for 1000 cycles and even shows good cycling performance (96.8% retention at 0.5 mA cm^{-2}) after 6000 cycles (Figure 3d, inset). In addition, the electrochemical impedance spectroscopy (EIS) data before and after cycling were compared (Supporting Information, Figure S4). The data showed that the resistance changed only slightly, further confirming the stability of the electrochemical performance.

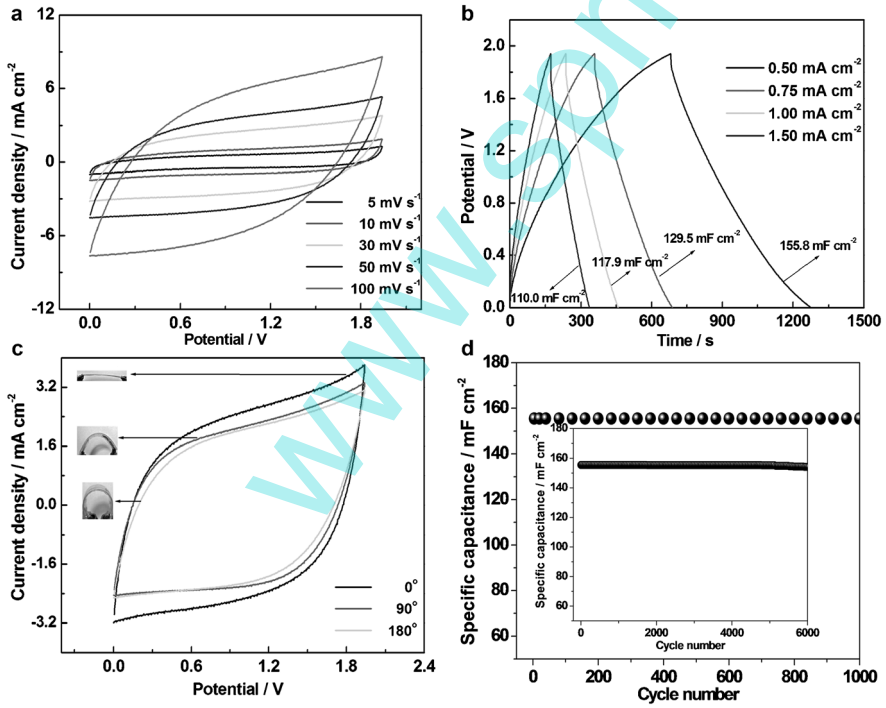

Figure 3. a) Cyclic voltammetry measurements carried out on the $CeVO_4$//graphene ASC device within the range of 0–1.9 V at a scan rate of 5–100 mV s^{-1}. b) Galvanostatic charge–discharge curves at current densities of 0.5–1.5 mA cm^{-2} and the corresponding specific capacitance. c) Cyclic voltammetry measurements within the range of 0–1.9 V at a scan rate of 30 mV s^{-1} carried out at different degrees of bending (0°, 90° and 180°). d) Cycle life performance tests at 0.5 mA cm^{-2}.

It is important to provide the reason for using $CeVO_4$ nanobelts in the as-prepared device. For comparison, we have also prepared $CeVO_4$ nanoparticles and microparticles (Supporting Information, Figure S5) by calcination at 500 °C and 700 °C, respectively. The $CeVO_4$ nanoparticles and microparticles are 10–70 nm and 1–2 μm in size. We have successfully assembled ASC devices as with $CeVO_4$ nanobelts//graphene nanosheets by using $CeVO_4$ nanoparticles/microparticles and graphene nanosheets. Galvanostatic charge–discharge curves of the three ASCs at a current density of 0.50 mA cm^{-2} are shown in Figure S2a in the Supporting Information. It is seen that the specific capacitance of the $CeVO_4$ nanobelts//graphene device is much larger than that of the other two ASCs. In fact, we have measured the performance of

the as-prepared three devices after 300 bending times with different bending angles (Supporting Information, Figure S2b). The specific capacitance of $CeVO_4$ nanoparticles//graphene and $CeVO_4$ microparticles//graphene decreased largely due to the poor mechanical and flexible properties of isolated $CeVO_4$ nanoparticles and microparticles. From the cycling life of the three devices (Figure S2c) one can see that the specific capacitance of the $CeVO_4$ nanobelts//graphene device retains 99.9% of the initial value, while that of $CeVO_4$ nanoparticles//graphene and $CeVO_4$ microparticles//graphene decreases to 81.4% and 68.8%. To rationalize these data, we have measured the electrochemical impedance spectra of the three devices at room temperature in the frequency range of 0.01–10^5 Hz under open-circuit conditions, as shown in Figure S2d in the Supporting Information. Furthermore, the charge-transfer resistance (R_{ct}) of the device was calculated by using the ZSimpWin software. The $CeVO_4$ nanobelts//graphene device has the lowest R_{ct} value of 10.5 Ω, while that of $CeVO_4$ nanoparticles//graphene and $CeVO_4$ microparticles//graphene is 59.5 and 113.0 Ω, respectively. The small charge-transfer resistance clearly demonstrates the reduced charge-transfer resistance of as-prepared $CeVO_4$ nanobelts, an effect possibly due to their structure, which may both decrease the electrode polarization and increase its electrochemical active sites.

The energy and power densities of the flexible solid-state ASCs measured in the potential window of 0–1.9 V at different scan rates are shown in Figure 4. Figure 4 also compares the volumetric power and energy densities of the $CeVO_4$ nanobelts//graphene ASC device reported in this work to the values reported for other energy storage devices. The as-fabricated ASC device has a maximum volumetric energy density of 0.78 mW h cm^{-3} at a current density of 0.5 mA cm^{-2}, and 0.55 mW h cm^{-3} at 1.5 mA cm^{-2}, again confirming the good rate performance of the $CeVO_4$ nanobelts//graphene ASC device. Moreover, the obtained maximum volumetric energy density is considerably higher than those of recently reported symmetric supercapacitor devices (SSCs)[13,35–38] and comparable to some developed ASCs,[23,39–43] such as TiO_2@MnO_2//TiO_2@C (0.30 mW h cm^{-3}, 0.5 mA cm^{-2}),[23] VO_x//VN (0.61 mW h cm^{-3}, 0.5 mA cm^{-2})[37] ZnO@MnO//graphene (0.234 mW h cm^{-3}, 0.5 mA cm^{-2})[40] MnO_2//Fe_2O_3 (0.41 mW h cm^{-3}, 0.5 mA cm^{-2}),[41] and Co_3O_4//graphene ASCs (0.62 mW h cm^{-3}, 20 mA cm^{-3}).[20] However, the obtained maximum volumetric energy density is lower than that of some previously reported ASCs.[39,43,44] Additionally, the $CeVO_4$//graphene ASC device can deliver a maximum power density of 118 mW cm^{-3} at a current density of 1.5 mA cm^{-2}, which is much higher than that of the recently reported ZnO@MnO_2 SSC,[38] polyaniline//WO_x@MoO_x ASC,[39] and ZnO@MnO_2//graphene ASC,[40] but lower than that of devices based on carbon materials or metal nitrides.[13,23,35,37] The results above confirm that the ultrathin $CeVO_4$ nanobelts are very promising as a high energy-density anode material for ASCs. To demonstrate the potential application of the $CeVO_4$ nanobelts//graphene ASC device, an ASC device was used to power a red light-emitting diode (LED) (Figure 4, inset). The ASC device can power a red LED (1.5 V) for about 2 min after charging at 1.5 mA cm^{-2} for 30 s.

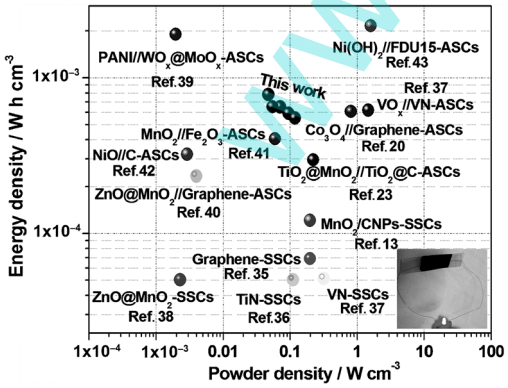

Figure 4. Ragone plots of the $CeVO_4$ nanobelts//graphene ASCs. The values reported for previous devices have been added for comparison.[13,23,35–43] Inset: A red LED (1.5 V) powered by the ultrathin $CeVO_4$ nanobelts//graphene ASC.

In summary, ultrathin $CeVO_4$ nanobelts have been successfully synthesized by a hydrothermal method. More importantly, a flexible solid-state asymmetric device has been successfully assembled by using the ultrathin $CeVO_4$ nanobelts and graphene. The assembled ultrathin $CeVO_4$ nanobelts//graphene ASCs achieve a maximum energy density of 0.78 mW h cm^{-3}, which is higher than that of most reported solid-state SCs, and can be efficiently cycled for 6000 cycles, which makes them one of the most promising candidates for high-performance flexible solid-state asymmetric supercapacitors in the field of energy storage devices. Other applications of these nanobelts are also anticipated by exploiting the advantages of flexibility and high energy density originating from both the architecture of the material and the novel design of the device. Further work is ongoing in our laboratory to improve the device performance and extend the scope of this work to other systems within the framework of flexible/stretchable energy devices.

Experimental Section

Synthesis of the $CeVO_4$ nanobelts

The $CeVO_4$ nanobelts were synthesized through a hydrothermal route from the reaction of $Ce(NO_3)_3$ and NH_4VO_3 in a Teflon-lined autoclave. All of the chemical reagents were of analytical grade and used without further purification. In a typical procedure, NH_4VO_3 (35.1 mg, 0.3 mmol) was dissolved in deionized water (25 mL) at 80 °C. Then $Ce(NO_3)_3{\cdot}6H_2O$ (200 mg, 0.46 mmol) was added, and the mixture was transferred into a 50 mL Teflon-lined autoclave and maintained at 200 °C for 5 h. After cooling to ambient temperature, the resulting yellow solid powder in the autoclave was collected by centrifugation, washed several times with deionized water and ethanol, and finally dried at 40 °C for 1 h in air.

Preparation of graphite oxide

Graphite oxide was produced from natural graphite powder (universal grade, 99.985%) according to the Hummers method. First, the graphite powder was treated twice with 5% HCl. It was then

filtered, washed thoroughly with distilled water, and dried at 110 °C for 24 h. Subsequently, the pre-treated graphite powder (10 g) was placed in cold (0 °C) concentrated H_2SO_4 (230 mL). Next, $KMnO_4$ (30 g) was added gradually with stirring and cooling, and the temperature of the solution was not allowed to go up to 20 °C. The mixture was stirred for 40 min, and distilled water (460 mL) was added slowly, resulting in an increase in temperature to 98 °C. The mixture was then cooled to 35±3 °C and maintained at this temperature for 30 min. Finally, distilled water (1.4 L) and 30% H_2O_2 solution (100 mL) were added to the reaction mixture. The solution was held at room temperature for 24 h and then the mixture was filtered, washed with 5% HCl aqueous solution until sulfate could not be detected with $BaCl_2$. The reaction product was dried under vacuum at 50 °C for 24 h.

Preparation of functionalized graphene sheets

The dried GO was thermally exfoliated at 300 °C for 5 min under air atmosphere. The obtained samples were subsequently heated to 700 °C in Ar for 3 h at a heating rate of 2 °C min^{-1}.

Characterizations

The morphology of as-prepared samples was observed by using a JEOL JSM-6701F field-emission scanning electron microscope (FE-SEM) at an acceleration voltage of 5.0 kV. The phase analyses of the samples were performed by X-ray diffraction (XRD) on a Rigaku-Ultima III with $Cu_{K\alpha}$ radiation (λ = 1.5418 Å). Transmission electron microscopy (TEM) images were captured on a JEM-2100 electron microscope at an acceleration voltage of 200 kV. Atomic force microscopy (AFM) images were measured using a CSPM4000 instrument (Benyuan, Beijing).

Fabrication and electrochemical study of the $CeVO_4$ nanobelt electrode in a conventional three-electrode system

All electrochemical performances were carried out on Arbin-BT6000 electrochemical instrument in a conventional three-electrode system equipped with a platinum electrode and a saturated calomel electrode (SCE) as counter and reference electrode, respectively. Before each electrochemical measurement, O_2 was purged out from the solution by the inert gas Ar. The working electrode was made from mixing of active materials—the $CeVO_4$ nanobelt electrode, acetylene black, and PTFE (polytetrafluoroethylene) with a weight ratio of 80:15:5, followed by coating on a piece of nickel foam of about 1 cm^2 and pressing it to a thin foil at a pressure of 5.0 MPa. The typical mass load of the electrode material was 5.0 mg. The electrolyte was 1.0 M LiCl solution. Galvanostatic charge-discharge methods were used to investigate capacitive properties of the ultrathin $CeVO_4$ nanobelt electrode, which were all carried out with an Arbin-BT6000 electrochemical instrument. Cyclic voltammetry measurements of the ultrathin $CeVO_4$ nanobelt electrode were conducted by using a PARSTAT2273 instrument.

Fabrication and electrochemical study of flexible solid-state ultrathin $CeVO_4$ nanobelts//graphene ASCs

The PET substrates (PET = polyethylene terephthalate) were first deposited with a layer of Pt film (ca. 3×5 nm thick) and then coated with the slurry containing the active materials (the ultrathin $CeVO_4$ nanobelts or graphene nanosheets) by a process similar to that in the three electrode system and were used as the working electrode after drying. In the meantime, the PVA/LiCl (PVA = polyvinyl alcohol) gel electrolyte was prepared as follows: the gel electrolyte (2.0 g PVA, 4.2 g LiCl, and 20 mL deionized water) was prepared by heating at 85 °C for 30 min under vigorous stirring (We have measured the PVA-LiCl gel-like and LiCl-H_2O electrolyte solution at different LiCl concentrations. In this work, the ionic conductivity of the gel-like electrolyte is 5.6 S m^{-1}, while that of 1.0 M LiCl solution is 5.2 S m^{-1}; Supporting Information, Figure S6). Subsequently, two pieces of such electrodes were immersed in the PVA/LiCl gel solution for 5–10 min to adsorb a layer of solid electrolyte. After the excess water was vaporized, two pieces of such electrodes containing electrolyte were pressed together on a sheet roller. Thus, the stacked all-solid-state ASCs were fabricated. CV measurements were carried out at 5, 10, 20, 30, 50, and 100 mV s^{-1} between 0 and 1.9 V on an electrochemical work station (PARSTAT-2273). The flexible solid-state $CeVO_4$//graphene ASCs were galvanostatically charged and discharged at a current density of 0.5–1.5 mA cm^{-2} in the voltage range of 0–1.9 V on an Arbin-BT6000 electrochemical instrument. All electrochemical measurements were conducted at room temperature.

Acknowledgements

This work is supported by New Century Excellent Talents of the University in China (grant no. NCET-13-0645) and National Natural Science Foundation of China (NSFC-21201010, U1304504), Program for Innovative Research Team (in Science and Technology) in University of Henan Province (14IRTSTHN004), the Science & Technology Foundation of Henan Province (14B150001).

Keywords: cerium orthovanadate · electrode materials · energy storage · supercapacitor · ultrathin nanobelts

[1] Y. G. Wang, Y. Y. Xia, *Electrochim. Acta* **2006**, *51*, 3223 – 3227.
[2] D. D. Zhao, M. W. Xu, W. J. Zhou, J. Zhang, H. L. Li, *Electrochim. Acta* **2008**, *53*, 2699 – 2705.
[3] S. L. Xiong, C. Z. Yuan, X. G. Zhang, B. J. Xi, Y. T. Qian, *Chem. Eur. J.* **2009**, *15*, 5320 – 5326.
[4] H. Pang, Z. Yan, W. Wang, J. Chen, J. S. Zhang, H. H. Zheng, *Nanoscale* **2012**, *4*, 5946 – 5953.
[5] H. Pang, Y. Y. Liu, J. Li, Y. H. Ma, G. C. Li, Y. N. Ai, J. Chen, J. S. Zhang, H. H. Zheng, *Nanoscale* **2013**, *5*, 503 – 507.
[6] H. Pang, Z. Yan, Y. Ma, G. Li, J. Chen, J. Zhang, W. Du, S. Li, *J. Solid State Electrochem.* **2013**, *17*, 1383 – 1391.
[7] X. H. Lu, G. M. Wang, T. Zhai, M. H. Yu, J. Y. Gan, Y. X. Tong, Y. Li, *Nano Lett.* **2012**, *12*, 1690 – 1696.
[8] Z. J. Fan, J. Yan, T. Wei, L. J. Zhi, G. Q. Ning, T. Y. Li, F. Wei, *Adv. Funct. Mater.* **2011**, *21*, 2366 – 2375.
[9] A. Lewandowski, A. Olejniczak, M. Galinski, I. Stepniak, *J. Power Sources* **2010**, *195*, 5814 – 5819.
[10] E. Frackowiak, *Phys. Chem. Chem. Phys.* **2007**, *9*, 1774 – 1785.
[11] K. W. Nam, C. W. Lee, X. Q. Yang, B. W. Cho, W. S. Yoon, K. B. Kim, *J. Power Sources* **2009**, *188*, 323 – 331.
[12] B. G. Choi, S. J. Chang, H. W. Kang, C. P. Park, H. J. Kim, W. H. Hong, S. G. Lee, Y. S. Huh, *Nanoscale* **2012**, *4*, 4983 – 4988.
[13] Z. B. Lei, J. T. Zhang, X. S. Zhao, *J. Mater. Chem.* **2012**, *22*, 153 – 160.
[14] H. C. Gao, F. Xiao, C. B. Ching, H. W. Duan, *ACS Appl. Mater. Interfaces* **2012**, *4*, 2801 – 2810.
[15] Z. S. Wu, W. C. Ren, D. W. Wang, F. Li, B. L. Liu, H. M. Cheng, *ACS Nano* **2010**, *4*, 5835 – 5842.
[16] J. Yan, Z. J. Fan, W. Sun, G. Q. Ning, T. Wei, Q. Zhang, R. F. Zhang, L. J. Zhi, F. Wei, *Adv. Funct. Mater.* **2012**, *22*, 2632 – 2641.
[17] Q. T. Qu, Y. Shi, L. L. Li, W. L. Guo, Y. P. Wu, H. P. Zhang, S. Y. Guan, R. Holze, *Electrochem. Commun.* **2009**, *11*, 1325 – 1328.
[18] W. H. Jin, G. T. Cao, J. Y. Sun, *J. Power Sources* **2008**, *175*, 686 – 691.

[19] X. H. Lu, T. Zhai, X. H. Zhang, Y. Q. Shen, L. Y. Yuan, B. Hu, L. Gong, J. Chen, Y. H. Gao, J. Zhou, Y. X. Tong, Z. L. Wang, *Adv. Mater.* **2012**, *24*, 938 – 944.
[20] X. F. Wang,, B. Liu, R. Liu, Q. F. Wang, X. J. Hou, D. Chen, R. M. Wang, G. Z. Shen, *Angew. Chem. Int. Ed.* **2014**, *53*, 1849 – 1853; *Angew. Chem.* **2014**, *126*, 1880 – 1884.
[21] Y. Cheng, H. Zhang, S. Lu, C. V. Varanasi, J. Liu, *Nanoscale* **2013**, *5*, 1067 – 1073.
[22] C. Z. Meng, C. H. Liu, L. Z. Chen, C. H. Hu, S. S. Fan, *Nano Lett.* **2010**, *10*, 4025 – 4031.
[23] X. H. Lu, M. H. Yu, G. M. Wang, T. Zhai, S. L. Xie, Y. C. Ling, Y. X. Tong, Y. Li, *Adv. Mater.* **2013**, *25*, 267 – 272.
[24] X. F. Wang, B. Liu, Q. F. Wang, W. F. Song, X. J. Hou, Y.-B. Cheng, G.-Z. Shen, *Adv. Mater.* **2013**, *25*, 1479 – 1486.
[25] C. Zhang, H. Yin, M. Han, Z. Dai, H. Pang, Y. Zheng, Y. Q. Lan, J. Bao, J. Zhu, *ACS Nano* **2014**, *8*, 3761 – 3770.
[26] Y. Zhang, Y. Liu, J. Chen, Q. F. Guo, T. Wang, H. Pang, *Sci. Rep.* **2014**, *4*, 5687 – 5687.
[27] a) X. Wang, Y. D. Li, *Angew. Chem. Int. Ed.* **2002**, *41*, 4790 – 4793; *Angew. Chem.* **2002**, *114*, 4984 – 4987; b) X. Wang, Y. D. Li, *Angew. Chem. Int. Ed.* **2003**, *42*, 3497 – 3500; *Angew. Chem.* **2003**, *115*, 3621 – 3624; c) Y. W. Zhang, X. Sun, R. Si, L. P. You, C. H. Yan, *J. Am. Chem. Soc.* **2005**, *127*, 3260 – 3261.
[28] a) J. F. Liu, Q. H. Yao, Y. D. Li, *Appl. Phys. Lett.* **2006**, *88*, 173119; b) J. F. Liu, Y. D. Li, *Adv. Mater.* **2007**, *19*, 1118 – 1122.
[29] C. H. Yan, L. D. Sun, C. S. Liao, Y. X. Zhang, Y. Q. Lu, S. H. Huang, S. Z. Lu, *Appl. Phys. Lett.* **2003**, *82*, 3511 – 3513.
[30] L. Y. Wang, R. X. Yan, Z. Y. Huo, L. Wang, J. H. Zeng, J. Bao, X. Wang, Q. Peng, Y. D. Li, *Angew. Chem. Int. Ed.* **2005**, *44*, 6054 – 6057; *Angew. Chem.* **2005**, *117*, 6208 – 6211.
[31] V. W. Yam, Q. Li, *Angew. Chem. Int. Ed.* **2007**, *46*, 3486 – 3489; *Angew. Chem.* **2007**, *119*, 3556 – 3559.
[32] a) J. Li, S. B. Tang, L. Lu, H. C. Zeng, *J. Am. Chem. Soc.* **2007**, *129*, 9401 – 9409; b) H. Ma, F. Y. Cheng, J. Chen, J. Z. Zhao, C. S. Li, Z. L. Tao, J. Liang, *Adv. Mater.* **2007**, *19*, 4067 – 4070; c) C. R. Sides, C. R. Martin, *Adv. Mater.* **2005**, *17*, 125 – 128.
[33] R. Tenne, *Nat. Nanotechnol.* **2006**, *1*, 103 – 111.
[34] a) P. L. Taberna, S. Mitra, P. Poizot, P. Simon, J. M. Tarascon, *Nat. Mater.* **2006**, *5*, 567 – 573; b) K. T. Nam, D. W. Kim, P. J. Yoo, C. Y. Chiang, N. Meethong, P. T. Hammond, Y. M. Chiang, A. M. Belcher, *Science* **2006**, *312*, 885 – 888.
[35] M. F. El-Kady, V. Strong, S. Dubin, R. B. Kaner, *Science* **2012**, *335*, 1326 – 1330.
[36] X. H. Lu, G. M. Wang, T. Zhai, M. H. Yu, S. L. Xie, Y. C. Ling, C. L. Liang, Y. X. Tong, Y. Li, *Nano Lett.* **2012**, *12*, 5376 – 5381.
[37] X. H. Lu, M. Yu, T. Zhai, G. Wang, S. Xie, T. Liu, C. Liang, Y. Tong, Y. Li, *Nano Lett.* **2013**, *13*, 2628 – 2633.
[38] P. Yang, X. Xiao, Y. Li, Y. Ding, P. Qiang, X. Tan, W. Mai, Z. Lin, W. Wu, T. Li, H. Jin, P. Liu, J. Zhou, C. P. Wong, Z. L. Wang, *ACS Nano* **2013**, *7*, 2617 – 2626.
[39] X. Xiao, X. Peng, H. Jin, T. Li, C. Zhang, B. Gao, B. Hu, K. Huo, J. Zhou, *Adv. Mater.* **2013**, *25*, 5091 – 5097.
[40] W. Zilong, Z. Zhu, J. Qiu, S. Yang, *J. Mater. Chem. C* **2014**, *2*, 1331 – 1336.
[41] X. H. Lu, Y. X. Zeng, M. H. Yu, T. Zhai, C. L. Liang, S. L. Xie, M.-S. Balogun, Y. X. Tong, *Adv. Mater.* **2014**, *26*, 3148 – 3155.
[42] L. N. Gao, X. F. Wang, Z. Xie, W. F. Song, L. J. Wang, X. Wu, F. Y. Qu, D. Chen, G. Z. Shen, *J. Mater. Chem. A* **2013**, *1*, 7168 – 7173.
[43] X. L. Dong, Z. Y. Guo, Y. F. Song, M. Y. Hou, J. Q. Wang, Y. G. Wang, Y. Y. Xia, *Adv. Funct. Mater.* **2014**, *24*, 3405 – 3412.
[44] D. S. Yu, K. Goh, H. Wang, L. Wei, W. C. Jiang, Q. Zhang, L. M. Dai, Y. Chen, *Nat. Nanotechnol.* **2014**, *9*, 555 – 562.

Received: September 16, 2014
Revised: October 12, 2014
Published online on November 19, 2014